Zentrum für Technomathematik
Fachbereich 3 – Mathematik und Informatik

A sharp-interface moving-boundary system modeling carbonation penetration in concrete

Adrian Muntean **Michael Böhm**

Report 06–03

Berichte aus der Technomathematik

Report 06–03 **April 2006**

A sharp-interface moving-boundary system modeling carbonation penetration in concrete

Adrian Muntean* Michael Böhm†

April 13, 2006

Abstract

We present a new way of modeling the penetration of the carbonation reaction front in concrete-based materials. The model consists of a two-phase moving-boundary system of weakly coupled parabolic equations to be solved together with a non-local ordinary differential equation, which describes the dynamics of the reaction interface. Simultaneously, we determine the position of the carbonation front and the active concentrations fields. The numerical method, outlined for this moving-boundary system, relies on two fixed-domain transformations and a suitable finite element Galerkin approach for the space discretization. The resulting non-local IVP is integrated in time using a stiff MATLAB odes solver. Our results have a twofold significance: on one hand, they contribute to the fundamental understanding of the complex dynamics of a fast reaction in non-saturated reactive porous materials, and on the other hand, they provide a sound basis for the efficient prediction of the location of the carbonation fronts in concrete.

Keywords: Moving-boundary problem, kinetic condition, concrete carbonation, reaction-diffusion systems, front-fixing technique, finite element method

1 Introduction

The need to design durable concrete structures in chemically aggressive environments leads to increasingly complex models and experiments to study deterioration phenomena. Concrete interacts with its environment. Some of these interactions usually induce deterioration processes which may initiate the corrosion of the steel reinforcement embedded in concrete. The two most common causes of reinforcement corrosion are (1) localized breakdown of the passive film on the steel by chloride and sulfate ions, e.g., and (2) general breakdown of passivity by decrease in pH (mainly due to the neutralization of dissolved $Ca(OH)_2$), predominantly by reaction with atmospheric CO_2. A concise introduction in the phenomenology of the concrete carbonation process is given in

*Centre for Industrial Mathematics, FB3(Mathematik und Informatik), Universität Bremen, Postfach 330440, 28334 Bremen, Deutschland (Germany), e-mail: muntean@math.uni-bremen.de

†Centre for Industrial Mathematics, FB3(Mathematik und Informatik), Universität Bremen, Postfach 330440, 28334 Bremen, Deutschland (Germany), e-mail: mbohm@math.uni-bremen.de

section 1.1. In order to emphasize the practical relevance of this problem, we mention that the increased use of de-icing salts and the increased concentration of CO_2 due to industrial pollution has resulted in corrosion of steel bars becoming the principal cause of concrete failure, see [14], e.g. Therefore, a challenge exists in ensuring a correct prediction of the internal corrosion, before costly damage is visually apparent on the facades of concrete structures.

It is our goal to contribute to a proper understanding of the natural carbonation of concrete in order to quantitatively predict and test, by models and validated experimental data, the long-term behavior of concrete-based materials under natural exposure conditions. For this purpose, we rely on the moving-boundary methodology (cf. [1, 23], e.g.) to tackle with this problem as opposed to the classical isolines approach typically employed in engineering applications (see [31, 22, 30], e.g.). Detailed surveys on the carbonation process in the context of durability *versus* corrosion issues are given in [14, 8] and chapter 2 of [26], e.g. In this paper, we propose a moving sharp-interface model for the carbonation of $Ca(OH)_2$, see section 1.1. The moving-boundary methodology can be successfully applied in this case if two model assumptions are satisfied: (a) The thin reaction zone, where the carbonation takes place (cf. reaction (1)), can be well approximated by a sharp (reaction) interface placed in its center; and (b) We assume that behind the reaction interface there is (almost) no $Ca(OH)_2$ left, or equivalently, we may consider that beyond the reaction interface there is no CO_2. The merit of this methodology is twofold: (i) Proper definitions of the reaction interface position and speed permit correct numerical predictions; (ii) Our formulation of the model allows for application of sophisticated adaptive solvers to our "fast reaction – slow diffusion" setting, see the pre-study [30] and references therein. On this way, the presence of complex geometries (like corners, e.g.) and the inherent occurrence of multiple characteristic time and length scales can be dealt with accurately. In this paper, we only discuss the case of the aggressive penetration of CO_2(g) into a finite 1D slab. Comparison of the simulated penetration depths with the measurements from [6] yields good agreement for a wide range of parameters. Other carbonation scenarios considering one or two moving-reaction zones (replacing moving-sharp interfaces) are discussed in [4, 5, 24] and analyzed in [26, 25]. Note also that a two-scale model for a reaction-diffusion process in a porous material was applied to a simplified carbonation scenario in [21]. Other modeling approaches concerning moving fast reaction fronts in non-saturated porous media have been done in the case of precipitation/dissolution reactions (see [20, 29, 11], e.g.), water front invading an unsaturated medium (see [12]), redox reactions (see [9], e.g.), gypsum formation in sewer pipes (see [3], e.g.) or when various reaction-induced instabilities occur in geochemistry (see [27], e.g.).

The paper has the following structure: In section 1.1 we concisely present the modeling details of the process, while in section 1.2 we describe the basic geometry we are taking into account as well as the main assumptions on the porosity and the volume fractions involved. The mathematical modeling via moving interfaces of a simplified carbonation scenario is the main topic of section 2. The immobilization of the moving interface and the numerical method, which we employ to solve the moving-boundary system in fixed domains, is discussed in section 3. Section 4 contains the results of our simulations used to recover experimental data from a real-life situation. The sharp-interface model proposed by this paper is succinctly evaluated in section 5.

1.1 Phenomenology of the process

Carbonation of concrete proceeds inwards from the exposed boundary. Atmospheric CO_2 enters the porous concrete and diffuses relatively fast through the air-filled parts of the pores and very slowly through the water-filled parts. At some distance from the outer surface it is consumed by the alkaline species (mainly $Ca(OH)_2$) which are available in the pore water via a dissolution mechanism that removes them from the solid parts which are in contact with water, see details in Fig. 1, but also [8, 6, 14, 28] and references therein. The carbon-

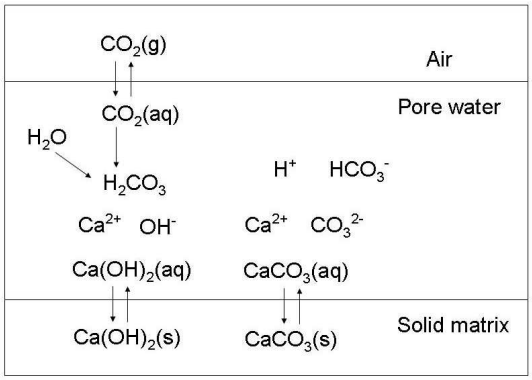

Figure 1: Ionic equilibrium in pore water cf. Ref. [19].

ation of $Ca(OH)_2$ is simply described by the following reaction mechanism:

$$CO_2(g \rightarrow aq) + Ca(OH)_2(s \rightarrow aq) \rightarrow CaCO_3(aq + s) + H_2O. \qquad (1)$$

Carbonation may or may not consume the available $Ca(OH)_2$. It can exhibit

(a) (b)

Figure 2: (a) Typical result of the phenolphthalein test on a partially carbonated sample (Courtesy of U. Dahme (AG Setzer), University of Duisburg-Essen, Germany). The dark region shows the uncarbonated part, while the brighter one points out the carbonated part. The two regions are separated by a sharp interface. (b) Definition of the interface position, see also Fig. 3 (b). Note that (a) and (b) are macroscopic pictures.

steep reaction fronts (here also called interfaces) or reaction zones. Particularly, the carbonation reaction (1) is very fast compared with the transport of CO_2 and, specifically, leads to the formation of a narrow internal reaction front which

travels through the material. Here, (1) is assumed to take place inside this front. The thin front separates the fully carbonated part from the yet uncarbonated part. Employing a concept used in the modeling of Stefan-like melting problems [1, 23], this separating layer remotely resembles to a "mushy" region. In this area connecting the carbonated and uncarbonated parts, reactants and products may not be segregated. The progress of this layer is the pattern of interest here. Its occurrence can be easily observed experimentally by spraying an indicator test (e.g. phenolphthalein) on a cut in the concrete sample, see Fig. 2 (a) and [8], e.g. The modeling, and hence, the calculation of its speed and position is the main scope of the paper. The formation of the layer can also be investigated, but we do not dwell on this aspect here.

1.2 Basic geometry. Assumptions on the choice of porosities

We consider a part Ω of the concrete sample depicted in Fig. 3 (a), which is exposed to ingress of CO_2(g) and humidity from the environment. The region Ω is chosen such that it contains the reaction front. Motivated by Fig. 2 (a) and (b), we idealize the reaction front by a surface $\Gamma(t)$. Let the positive x-axis be directed normally to $\Gamma(t)$ and into the uncarbonated part. The basic geometry is sketched in Fig. 3. At $t = 0$, we assume that the origin located at $x = 0$ is behind the reaction interface $\Gamma(t)$. Assuming that the reactants, which depend only on the real variables x and t, are available for reaction, we expect that the reaction interface moves as $x = s(t)$ for $t \in S_T :=]0, T[$ such that $s(0) = s_0$, where $T > 0$, $s_0 \in]0, L[$, and $L > 0$ are given, see Fig. 3 (b). We assume that beyond this front there is no CO_2 left (Fig. 2 (b)). Due to

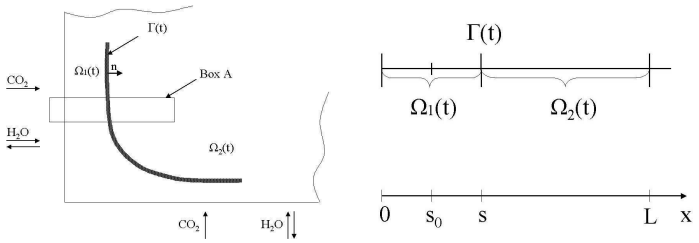

(a) (b)

Figure 3: (a) Basic geometry in the moving sharp-interface model. The box A is the region which our model refers to. (b) Schematic 1D geometry. The reactants are spatially segregated at any time t.

the heterogeneity of the concrete, the region Ω always consists of two distinct parts Ω_p and Ω_s. The part Ω_p represents the inner pores space, and Ω_s is the part occupied by the consolidated aggregate and mortar. We denote by ϕ the volumetric total[1] porosity. This quantity is defined as the ratio of volume of the pores space, which we denote by $|\Omega_p|$, to the bulk volume $|\Omega|$ of the control

[1] Cf. [2], p.44, when Ω_p is the total pore space, regardless of whether the pores are interconnected or not, or whether dead-end pores and fractures are present, the porosity ϕ is referred to as *total* porosity.

concrete region, see [2]. For most usual cement-based materials (like Ordinary Portland Concrete (OPC), for instance cf. [28]), the porosity $\phi = \frac{|\Omega_p|}{|\Omega|}$ has a value of about 0.2. For instance, cf. Ref. [28], the initial concrete porosity ϕ_0 can be sufficiently well described by

$$\phi_0 := \frac{R_{w/c}\frac{\rho_c}{\rho_w}}{\left(R_{w/c}\frac{\rho_c}{\rho_w} + R_{a/c}\frac{\rho_c}{\rho_a} + 1\right)}, \tag{2}$$

where $R_{w/c}$ and $R_{a/c}$ represent the water-to-cement and aggregate-to-cement ratios, while ρ_a, ρ_w and ρ_c are aggregate, water and concrete densities. Furthermore, we introduce the notion of volume fractions, that is we define the quantities

$$\phi_a = \frac{|\Omega_a|}{|\Omega_p|},\ \phi_w = \frac{|\Omega_w|}{|\Omega_p|} \text{ and } \phi_s = \frac{|\Omega_s|}{|\Omega|} \tag{3}$$

to be the air, water and solid fractions, respectively. In (3), $|\Omega_a|$ is the volume of the air-filled parts of the pores space, $|\Omega_w|$ is the volume of the respective water-filled parts and $|\Omega_s|$ denotes the volume of the solid matrix. It holds that $\phi_a + \phi_w = 1$ and $\phi\phi_a + \phi\phi_w + \phi_s = 1$. We tacitly assume that the averaged areal porosity is the same as the averaged volume porosity (cf. [18], p.31 or [2], p.22).

2 The sharp-interface carbonation model

We denote the mass concentration of the reactants and products as follows: $\bar{u}_1 := [CO_2(aq)]$, $\bar{u}_2 := [CO_2(g)]$, $\bar{u}_4 := [CaCO_3(aq)]$ and $\bar{u}_5 := [H_2O]$ are the chemical species present in the region $\Omega_1(t) := [0, s(t)[$; $\bar{u}_3 := [Ca(OH)_2(aq)]$ and $\bar{u}_6 := [H_2O]$ are species present in $\Omega_2(t) :=]s(t), L]$. Here, $\bar{u}_5$ and $\bar{u}_6$ refer to the water produced via (1). We assume that the rest of the humidity existing in the concrete does not affect the carbonation process. In other words, the material is considered to be almost dry, but however, a certain humidity level is needed to facilitate (1). We use the set of indices $\mathcal{I} := \mathcal{I}_1 \cup \{4\} \cup \mathcal{I}_2$, where $\mathcal{I}_1 := \{1, 2, 5\}$ points out the active concentrations in $\Omega_1(t)$ and $\mathcal{I}_2 := \{3, 6\}$ refers to the active concentrations living in $\Omega_2(t)$. Once built up, carbonates quickly precipitate to the solid matrix. We assume that $CaCO_3(aq)$ is not transported in $\Omega := \Omega_1(t) \cup \Gamma(t) \cup \Omega_2(t)$, therefore the only partly dissipative character of the model. Then, we are led to discuss the *moving-boundary problem* of determining the concentrations $\bar{u}_i(x,t), i \in \mathcal{I}$ and the interface position $s(t)$ which satisfy for all $t \in S_T$ the equations

$$\begin{cases} \left(\phi\phi_w\nu_{i2}\bar{u}_i\right)_{,t} + \left(-D_i\nu_{i2}\phi\phi_w\bar{u}_{i,x}\right)_x &=& f_{i,Henry}, \quad x \in \Omega_1(t), i \in \{1,2\}, \\ \left(\phi\phi_w\bar{u}_3\right)_{,t} + \left(-D_3\phi\phi_w\bar{u}_{3,x}\right)_x &=& f_{Diss}, \quad x \in \Omega_2(t), \\ \left(\phi\phi_w\bar{u}_4\right)_{,t} &=& f_{Prec} + f_{Reac\Gamma}, \quad x = s(t) \in \Gamma(t), \\ \left(\phi\bar{u}_5\right)_{,t} + \left(-D_5\phi\bar{u}_{5,x}\right)_x &=& 0, \quad x \in \Omega_1(t), \\ \left(\phi\bar{u}_6\right)_{,t} + \left(-D_6\phi\bar{u}_{6,x}\right)_x &=& 0, \quad x \in \Omega_2(t). \end{cases} \tag{4}$$

A derivation via first principles of the mass-balances (4) is given in [26]. The initial and boundary conditions are $\phi\phi_w\nu_{i2}\bar{u}_i(x,0) = \hat{u}_{i0}$, $i \in \mathcal{I}, x \in \Omega(0)$,

$\phi\phi_w\nu_{i2}\bar{u}_i(0,t) = \lambda_i$, $i \in \mathcal{I}_1$, $\bar{u}_{i,x}(L,t) = 0$, $i \in \mathcal{I}_2$, where $t \in S_T$. Specific to our problem, we impose the following interface conditions

$$\left\{ \begin{array}{lcl} [j_1 \cdot n]_{\Gamma(t)} & = & -\tilde{\eta}_\Gamma(s(t),t) + s'(t)[\phi\phi_w \bar{u}_1]_{\Gamma(t)}, \\ [j_i \cdot n]_{\Gamma(t)} & = & \tilde{\eta}_\Gamma(s(t),t)\delta_{5i} + s'(t)[\phi\phi_w \nu_{i2}\bar{u}_i]_{\Gamma(t)}, \quad i \in \{2,5,6\}, \\ [j_3 \cdot n]_{\Gamma(t)} & = & -\tilde{\eta}_\Gamma(s(t),t) + s'(t)[\phi\phi_w \bar{u}_3]_{\Gamma(t)}, \end{array} \right. \tag{5}$$

together with the differential equation

$$s'(t) = \alpha \frac{\tilde{\eta}_\Gamma(s(t),t)}{\phi\phi_w \bar{u}_3(s(t),t)} \text{ with } s(0) = s_0. \tag{6}$$

In (4)-(6), we select $\nu_{12} = \nu_{32} := 1$, $\nu_{22} := \frac{\phi_a}{\phi_w}$, $\nu_{52} = \nu_{62} := \frac{1}{\phi_w}$, $\nu_{i\ell} := 1$ $(i \in \mathcal{I}, \ell \in \mathcal{I} - \{2\})$, $\alpha > 0$ and $s_0 > 0$. Moreover, δ_{ij} $(i,j \in \mathcal{I})$ is Kronecker's symbol and $j_i := -D_i\nu_{i\ell}\phi\phi_w\bar{u}_i$ $(i,\ell \in \mathcal{I}_1 \cup \mathcal{I}_2)$ are the corresponding Fickian diffusive fluxes. Here D_i and L are strictly positive constants. The Dirichlet boundary data λ_i are prescribed in agreement with the environmental conditions to which Ω - a part of a concrete sample (cf. Fig. 3 (b)) - is exposed. The initial conditions $\hat{u}_{i0} > 0$ are determined by the chemistry of the cement, see [4]. The hardened mixture of aggregate, cement and water (i.e. the concrete) imposes ranges for the porosity $\phi > 0$ and also for the water and air fractions, $\phi_w > 0$ and $\phi_a > 0$, see section 1.2. Since the active concentrations are small, the constant porosity assumption is valid. The productions terms $f_{i,Henry}$, f_{Diss}, f_{Prec} and $f_{Reac\Gamma}$ are sources or sinks by transfer mechanisms at water-liquid interfaces inside the pores (e.g. via Henry's law, see [18], p.40), dissolution, precipitation and carbonation reactions. Here we set

$$\left\{ \begin{array}{l} f_{i,Henry} := (-1)^i P_i(\phi\phi_w\bar{u}_1 - Q_i\phi\phi_a\bar{u}_2)(P_i > 0, Q_i > 0), i \in \{1,2\}, \\ f_{Diss} := -S_{3,diss}(\phi\phi_w\bar{u}_3 - u_{3,eq}), S_{3,diss} > 0, f_{Prec} := 0, f_{Reac\Gamma} := \sigma\tilde{\eta}_\Gamma. \end{array} \right. \tag{7}$$

Specifically, $f_{i,Henry}$ and f_{Diss} model deviations from local equilibrium configurations (see chapters 2 and 6 in [10], e.g.) and f_{Prec} points out an instantaneous source of precipitation. While $f_{i,Henry}$ and f_{Diss} are linear production terms, $f_{Reac\Gamma}$ is usually non-linear. Owing to (7), we note that the production by reaction $f_{Reac\Gamma}$ is proportional to σ and $\tilde{\eta}_\Gamma$, where σ is the corresponding stoichiometric coefficient and the term $\tilde{\eta}_\Gamma$ denotes the carbonation reaction rate. For the stoichiometric configuration of (1), we have $\sigma = 1$. We define $\tilde{\eta}_\Gamma$ in the following fashion: Let $\bar{u}$ denote the vector of concentrations $(\bar{u}_1, \ldots, \bar{u}_6)^t$ and M_Λ be the set of parameters $\Lambda := (\Lambda_1, \ldots, \Lambda_m)^t$ that are needed to describe the reaction rate. For our purposes, it suffices at this moment to assume that M_Λ is a non-empty compact subset of $\mathbb{R}^m_+$. We introduce the function

$$\bar{\eta}_\Gamma : \mathbb{R}^6 \times M_\Lambda \to \mathbb{R}_+ \text{ by } \bar{\eta}_\Gamma(\bar{u}(x,t),\Lambda) := k\phi\phi_w\bar{u}_1^p(x,t))\bar{u}_3^q(x,t), x = s(t). \tag{8}$$

In (8), $m := 3$ and $\Lambda := \{p, q, k\phi\phi_w\} \in \mathbb{R}^3_+$ present a generalized mass-action law. We define the reaction rate $\tilde{\eta}_\Gamma(s(t),t)$ by $\tilde{\eta}_\Gamma(s(t),t) := \bar{\eta}_\Gamma(\bar{u}(s(t),t), \Lambda)$, where $\bar{\eta}_\Gamma$ is given by (8) and represents the classical power-law ansatz [10]. We specifically assume that $\bar{\eta}_\Gamma > 0$ if $\bar{u} > 0$ and $\bar{\eta}_\Gamma = 0$, otherwise. Furthermore, note that some equations act in $\Omega_1(t)$, while others act in $\Omega_2(t)$ or at $\Gamma(t)$. All of the three space regions are varying in time and they are *a priori* unknown.

Remark 2.1 (On the conditions across the moving interface) *The interface conditions (5) and (6) require further explanation. The term* $\tilde{\eta}_\Gamma(s(t),t) \approx \frac{1}{\alpha}s'(t)$ *denotes the number of moles per volume that is transported by diffusion to the interface* $\Gamma(t)$*. On the other hand, the proportionality* $s'(t) \approx \frac{1}{\phi\phi_w \bar{u}_3(s(t),t)}$ *emphasizes that the speed* s' *decreases as the amount of* $\mathrm{Ca(OH)_2}(aq)$ *near* $\Gamma(t)$ *increases. The expression* $\pm\phi\phi_w\bar{u}(s(t),t)s'(t)$ *accounts for the mass flux induced by the motion of* $\Gamma(t)$ *in order to preserve the conservation of mass. The conditions (5) express jumps in the gradients of concentrations across* $\Gamma(t)$*. They are typical interface relations for a surface-reaction mechanism and can be derived by applying the pillbox lemma (cf. [13], e.g.), see also the classical Rankine-Hugoniot jump relations in [1], section 1.2.E, e.g. The non-local law (6) governs the dynamics of the reaction interface. The latter interface condition is derived via first principles in the 1D case and for simple 2D geometries in [26]. It is needed to close the model formulation and allows the exact determination of the interface location once the reactants at* $\Gamma(t)$ *are known. The setting is applicable when the reaction rate* $\tilde{\eta}_\Gamma$ *is very fast compared to the diffusion of the gaseous* $\mathrm{CO_2}$*, or in other terms, when the characteristic time of the carbonation reaction is much smaller than the characteristic time of diffusion of the fastest species. This difference in the characteristic times causes the concentrations of the active chemical species and their gradient to have a jump at* $\Gamma(t)$*. The magnitude of the jump typically depends on the concentration itself.*

The system (4)-(8) forms the *sharp-interface carbonation model* P_Γ. The model P_Γ consists of a coupled semi-linear system of parabolic equations that has a moving *a priori* unknown internal boundary $\Gamma(t)$, where the carbonation reaction is assumed to take place. The coupling between the equations and the non-linearities comes from the influence of the chemical reaction on the transport part and also from the dependence of the moving regions $\Omega_1(t)$ and $\Omega_2(t)$ on $s(t)$. Other non-linearities may be introduced by different assumptions on the production terms.

Remark 2.2 (Well-posedness of P_Γ**)** *In [25] (Theorem* 2.2 *and Theorem* 2.6*) and [26], the global existence and uniqueness of weak solutions to* P_Γ *are addressed when some size restrictions on data and model parameters are satisfied. Furthermore, under alike circumstances the weak solution is also stable with respect to small changes in the initial data and model parameters.*

3 Simulation

3.1 Front-fixing approach

We reformulate the model P_Γ, that is (4)-(8), in terms of macroscopic quantities by performing the transformation of all concentrations into volume-based concentrations via $\hat{u}_i := \phi\phi_w\bar{u}_i, i \in \{1,3,4\}, \hat{u}_2 := \phi\phi_a\bar{u}_2, \hat{u}_i := \phi\bar{u}_i, i \in \{5,6\}$ and map P_Γ onto a domain with fixed boundaries. To this effect, we employ Landau-like transformations similar to those employed, for instance, in [16, 15, 12]. Let $t \in S_T$ be arbitrarily fixed. We have $(x,t) \in [0,s(t)] \times \bar{S}_T \longmapsto (y,\tau) \in [0,1] \times \bar{S}_T$, $y = \frac{x}{s(t)}$ and $\tau = t$, for $i \in \mathcal{I}_1$, $(x,t) \in [s(t),L] \times \bar{S}_T \longmapsto (y,\tau) \in [1,2] \times \bar{S}_T$, $y = 1 + \frac{x-s(t)}{L-s(t)}$ and $\tau = t$, for $i \in \mathcal{I}_2$. We label τ by t and introduce the new

concentrations, which act in the auxiliary y-t plane by $u_i(y,t) := \hat{u}_i(x,t) - \lambda_i(t)$ for all $i \in \mathcal{I}_1 \cup \mathcal{I}_2$. Thus, the model equations are reduced to

$$(u_\ell + \lambda_\ell)_{,t} - \frac{1}{s^2(t)}(D_\ell u_{\ell,y})_{,y} = f_\ell(u+\lambda) + y\frac{s'(t)}{s(t)}u_{\ell,y}, \tag{9}$$

$$(u_r + \lambda_r)_{,t} - \frac{1}{(L-s(t))^2}(D_i u_{r,y})_{,y} = f_r(u+\lambda) + (2-y)\frac{s'(t)}{L-s(t)}u_{r,y}, \tag{10}$$

where $\ell \in \mathcal{I}_1$, $r \in \mathcal{I}_2$, u is the vector of concentrations $(u_1, u_2, u_3, u_5, u_6)^t$ and λ represents the boundary data $(\lambda_1,\lambda_2,\lambda_3,\lambda_5,\lambda_6)^t$. We make use of λ_3 and λ_6 only for formal notational reasons ($\lambda_3 := \lambda_6 := 0$). The transformed initial, boundary and interface conditions are

$$u_i(y,0) = u_{i0}(y), i \in \mathcal{I}_1 \cup \mathcal{I}_2, u_i(a,t) = 0, i \in \mathcal{I}_1, u_{i,y}(b,t) = 0, i \in \mathcal{I}_2, \tag{11}$$

$$\frac{-D_1}{s(t)}u_{1,y}(1) = \eta_\Gamma(1,t) + s'(t)(u_1(1) + \lambda_1), \tag{12}$$

$$\frac{-D_2}{s(t)}u_{2,y}(1) = s'(t)(u_2(1) + \lambda_2), \tag{13}$$

$$\frac{-D_3}{L-s(t)}u_{3,y}(1) = -\eta_\Gamma(1,t) + s'(t)(u_3(1) + \lambda_3), \tag{14}$$

$$\frac{-D_5}{s(t)}u_{5,y}(1) + \frac{D_6}{L-s(t)}u_{6,y}(1) = \eta_\Gamma(1,t), u_5(1) + \lambda_5 = u_6(1) + \lambda_6, \tag{15}$$

where $\eta_\Gamma(1,t)$ denotes the reaction rate that acts in the y-t plane. This is defined by

$$\eta_\Gamma(1,t) := \bar{\eta}_\Gamma(\bar{u}(ys(t),t) + \lambda(t), \Lambda), y \in [0,1], \tag{16}$$

for given $\Lambda \in M_\Lambda$ and $\bar{\eta}_\Gamma$ cf. (8). We also mention that $u_{i0}(y) = \hat{u}_{i0}(x) - \lambda_i(0)$, where $x = ys_0$, $y \in [0,1]$ for $i \in \mathcal{I}_1$, and $x = s_0 + (y-1)(L-s_0)$, $y \in [1,2]$ for $i \in \mathcal{I}_2$. Finally, two odes

$$s'(t) = \eta_\Gamma(1,t) \text{ and } v_4'(t) = f_4(v_4(t)) \text{ a.e. } t \in S_T, \tag{17}$$

where $v_4(t) := \hat{u}_4(s(t),t)$ for $t \in S_T$, complete the model formulation. We also assume the strict positivity of their initial values

$$s(0) = s_0 > 0, v_4(0) = \hat{u}_{40} > 0. \tag{18}$$

The transformed model equations are collected in (9)-(18).

3.2 Numerical method

To perform the simulations, we employ a Galerkin scheme (cf. chapter 10 in [17], e.g.), in which the space discretization is done by standard linear finite elements. The procedure yields a system of odes which can then be integrated by one of the readily available MATLAB odes integrators. We use $n = 80$ grid points to discretize uniformly each of the fixed regions. The uniformity of the mesh indicates that a relatively large number of grid points is required to approximate

the dynamics of the moving interface. We define piecewise linear spline functions on the interval $[0,1]$ with respect to the uniform mesh $\left[0, \frac{1}{n}, \frac{2}{n}, \ldots, \frac{n-1}{n}, 1\right]$ by

$$\psi_{ij}^n(y) := \begin{cases} 1-|ny-j|, & \text{if } y \in \left[\frac{j-1}{n}, \frac{j+1}{n}\right] \cap [0,1] \\ 0, & \text{elsewhere on } [0,1]\ , \end{cases}$$

where $i \in \mathcal{I}$ and $j \in \mathcal{J} := \{1, \ldots, n\}$. We also need some additional notations:

$$U_i^n(t) := [U_{i1}^n(t), U_{i2}^n(t), \ldots, U_{in}^n(t)]^t \in \mathbb{R}_+^n \ (i \in \mathcal{I}), t \in S_T,$$

$$\psi_i^n(y) := [\psi_{i1}^n(y), \psi_{i2}^n(y), \ldots, \psi_{in}^n(y)]^t \in \mathbb{R}^n \ (i \in \mathcal{I}),$$
$$\Lambda_i^n := [\Lambda_i, \ldots, \Lambda_i]^t \in \mathbb{R}_+^n \ (i \in \mathcal{I}),\ \mathbb{I}_n := (1, \ldots, 1)^t \in \mathbb{R}^n.$$

To write the Galerkin system, we make use of the mass and stiffness matrices as well as of two additional matrices arising from the use of Landau transformations. The matrices M^n, K^n, L_l^n and L_r^n are given by $[M^n]_{ij} := \int_0^1 \psi_i^n(y)\psi_j^n(y)dy$, $[K^n]_{ij} := \int_0^1 \psi_i^{n\prime}(y)\psi_j^{n\prime}(y)dy$, $[L_l^n]_{ij} := \int_0^1 y\psi_i^n(y)\psi_j^{n\prime}(y)dy$, $[L_r^n]_{ij} := \int_0^1 (2-y)\psi_i^n(y)\psi_j^{n\prime}(y)dy$, see [3, 4] for their calculation. Let us assume

$$u_{in}(y,t) := U_i^n(t)\,[\psi_i^n(y)]^t = \sum_{j=1}^n U_{ij}^n(t)\psi_{ij}^n(y) \ (i \in \mathcal{I}).$$

We write the Galerkin system in terms of the basis $\{\psi_{ij}^n\}$ for all $(i,j) \in \mathcal{I} \times \mathcal{I}$ as follows:

$$M^n \frac{dU_i^n(t)}{dt} = -\frac{D_i K^n U_i^n(t)}{s_n(t)^2} + \frac{s_n'(t)}{s_n(t)} L_2^n U_i^n(t) + G_{in} \ (i \in \mathcal{I}_1 \cup \{4\}), \quad (19)$$

$$M^n \frac{dU_i^n(t)}{dt} = -\frac{D_i K^n U_i^n(t)}{(L-s_n(t))^2} + \frac{s_n'(t)}{(L-s_n(t))} L_r^n U_i^n(t) + G_{in} \ (i \in \mathcal{I}_2), \quad (20)$$

where the speed of the reaction interface $\Gamma(t)$ is approximated by

$$s_n'(t) = \alpha k \frac{(U_{1n}^n(t) + \Lambda_1^n)^p\,(U_{3n}^n(t) + \Lambda_3^n)^q}{U_{3n}^n(t) + \Lambda_3^n} \quad (21)$$

for each $t \in S_T$ such that $s_n(0) = s_0$. The discrete production terms $G_{in}(\cdot)$ arising in (19) are now given by

$$\begin{cases} G_{1n} := -P_1\left[Q_1 M^n U_{1n}^n(t) - M^n U_{2n}^n(t) + Q_1\Lambda_1^n - \Lambda_2^n\right], \\ G_{2n} := P_2\left[Q_2 M^n U_{1n}^n(t) - M^n U_{2n}^n(t) + Q_2\Lambda_1^n - \Lambda_2^n\right] \\ \qquad - k\,(U_{1n}^n(t) + \Lambda_1^n)^p\,(U_{3n}^n(t) + \Lambda_3^n)^q, \\ G_{3n} := S_{3,Diss}\left[u_{3,eq}^n - M^n U_{3n}^n(t) - \Lambda_3^n\right], \\ \qquad - k\,(U_{1n}^n(t) + \Lambda_1^n)^p\,(U_{3n}^n(t) + \Lambda_3^n)^q, \\ G_{4n} := k\,(U_{1n}^n(t) + \Lambda_1^n)^p\,(U_{3n}^n(t) + \Lambda_3^n)^q, G_{5n} := G_{6n} := 0, \end{cases} \quad (22)$$

where the discrete macroscopic equilibrium concentration of $Ca(OH)_2$ is defined by $u_{3,eq}^n := \mathbb{I}_n u_{3,eq}$ with $\mathbb{I}_n := (1, \ldots, 1)^t \in \mathbb{R}^n$.

We associate to the initial-value problem (19)-(22) the initial conditions

$$U_i^n(0) = 0 \text{ for all } i \in \mathcal{I} \text{ and } s_n(0) = s_0 > 0. \quad (23)$$

The non-local initial-value problem in its matrix form (19)-(22) has a unique locally in time solution provided the initial conditions (23) and some restrictions on the model parameters (like $p \geq 1$, $q \geq 1$ and so on) are fulfilled.

Remark 3.1 *We expect that some ideas from [12] and [7] can be adapted to our setting in order to point out that for large values of n the discrete approximations u_{in} ($i \in \mathcal{I}$) and s_n converge (in a certain sense) to u_i ($i \in \mathcal{I}$), and respectively to s. We do not cope with these aspects here.*

4 Simulation results and discussion

The numerical results are obtained based on the parameters specified in Table 1 and Table 2 and those explained in the sequel. For convenience, we set $\lambda_i = u_{0i}$ ($i \in \mathcal{I}_1 \cup \{4\}$) , $u_{05} = u_{06}$, $D_5 = D_6$, $P_1 = P_2 = P$, $Q_1 = Q_2 = Q$ and $\alpha = \mathcal{M}^{q-1}_{Ca(OH)_2}\mathcal{M}^{p}_{CO_2}$, where $\mathcal{M}_E$ denotes the molecular weight of the species E and p, q are the partial orders of reaction. To calculate λ_1 and λ_2, we split via Henry's law the ambient concentration of CO_2, say $\bar{c}$, which is present at the exposed boundary, i.e. $(\lambda_1, \lambda_2) = \left(\frac{\bar{c}Q}{1+Q}, \frac{\bar{c}}{1+Q}\right)$, see [4]. Another possible choice is $(\lambda_1, \lambda_2) = (0, \bar{c})$. The initial value of $CaCO_3$(aq) is given by $\hat{u}_{40} = \bar{k}\hat{u}^p_{10}\hat{u}^q_{30}$, where $\bar{k} \approx 500$. This means that at the beginning of the carbonation process, some amount of carbonates is already present. An alternative choice is $\hat{u}_{40} = 0$. Furthermore, to keep the numerical approach as simple as possible, we add in (19) a small artificial diffusion term (with $D_4 = 10^{-6}$ cm^2 day^{-1}) to the equation describing the evolution of $CaCO_3(aq)$. If we are interested in calculating the macroscopic concentration profiles and position of the macroscopic reaction interface, then explicit values of the porosity ϕ and material fractions ϕ_w and ϕ_a are not necessary. If however, we want to explore the microscopic information, then some information about the size of ϕ_w and ϕ_a is needed. In this section, we only plot the macroscopic concentration profiles. For instance, taking $\phi_w = 1 - \phi_a = 10\%$ and ϕ cf. (2), we can easily obtain typical concentration profiles of the active species at the pore level.

We consider an 18 years old concrete wall made of the cement PZ35F, whose chemistry, microstructure and outdoor exposure conditions are described in Table 3.1 of [6]. Since we are not aware of experimental values for all needed parameters, some values (like those for ϕ_w, P and $S_{3,diss}$) are theoretical. All parameters are considered constant throughout the carbonated and uncarbonated regions. The purpose of the numerical simulations is to identify the relevant parameters and their role in the carbonation process.

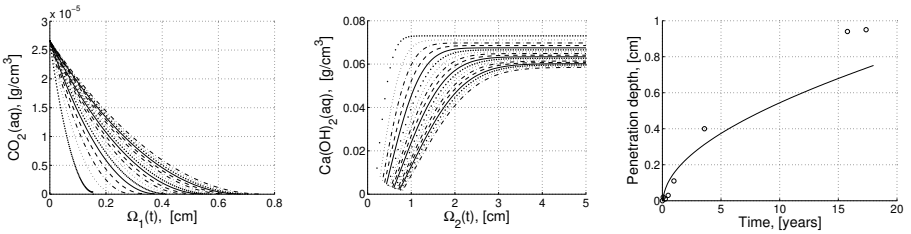

(a) (b) (c)

Figure 4: (a)+(b) CO_2(aq) and $Ca(OH)_2$(aq) profiles *vs.* space. Each curve refers to time $t = i$ years, $i \in \{1, \ldots, 18\}$. (c): Interface position *vs.* the experimental points " $\circ$ " after $T = 18$ years of exposure.

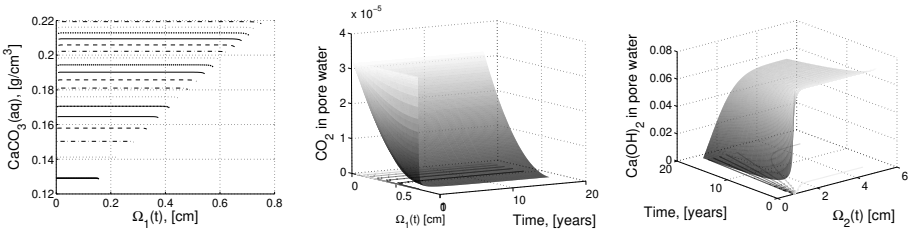

(a) (b) (c)

Figure 5: (a) $CaCO_3$(aq) profiles *vs.* space. Each curve refers to time $t = i$ years, $i \in \{1, \ldots, 18\}$. (b)+(c) Concentration of CO_2(aq) and $Ca(OH)_2$(aq) *vs.* time and space.

The plots in Fig. 4–5 show the solution of the P_Γ model. Since during the time interval S_T only small changes appear in the concentration profiles of water produced via (1), we omit to show the corresponding profiles, which are almost constant. Observe that steep $Ca(OH)_2$-concentration gradients arise near $\Gamma(t)$ (cf. Fig. 4 (b), Fig. 5 (c), e.g.). The calculated interface location is in the experimental range, see Fig. 4 (c) and Fig. 6.

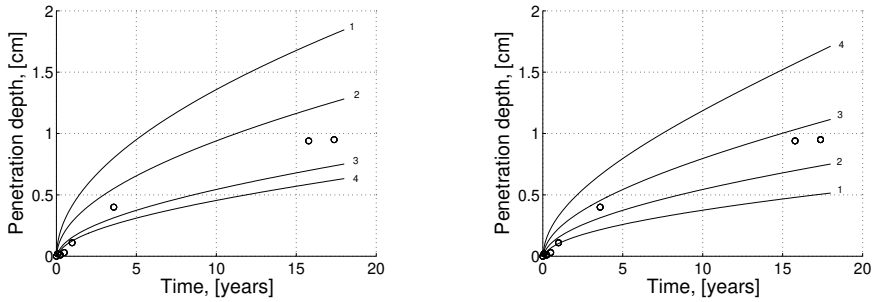

(a) (b)

Figure 6: (a) Interface location *vs.* the experimental points " ∘ " when varying the partial reaction order $p = 1.5, 1.3, 1, 0.9$ while $q = 1$. (b) Interface location *vs.* the experimental points " ∘ " when varying the effective dimensional diffusion coefficient of CO_2(g) as follows: $\frac{D_2}{2}$, D_2, $2D_2$ and $4D_2$.

Furthermore, Fig. 5 (a) shows a gradual increase in the concentration of $CaCO_3$(aq) within $\Omega_1(t)$. It visualizes the expansion of $\Omega_1(t)$ and also points out the shrinking of $\Omega_2(t)$. The results in Fig. 6 indicate a strong dependence of the penetration speed on the structure of the reaction rate $\tilde{\eta}_\Gamma$ and on the range of the effective diffusion coefficient of CO_2(g). Changing the exponent p from 0.9 to 1.5 produces a significant increase of the reaction rate, which finally results in a higher penetration depth. The penetration depth obtained with $p = 1.5$ is at least twice bigger than that obtained for $p = 1$ (compare the curve 1 with the curve 4 in Fig. 6 (a)). Alterations of the exponent q may lead to drastic changes in the penetration depth as well. An increase in the effective diffusivity of CO_2(g) produces a significant increase in the penetration depth.

Owing to Fig. 6 (b), the tendency is clear: If CO_2(g) encounters difficulties

Quantity	*Definition*	*Dimension*	*Value*
$R_{w/c}$	Water:cement ratio	-	0.60
$R_{a/c}$	Aggregate:cement ratio	-	5.1429
ρ_c	Cement density	g cm^{-3}	3.15
ρ_a	Aggregate density	g cm^{-3}	2.7

Table 1: Material characteristics of the concrete sample, [4, 6].

to travel to the reaction zone, then the speed of the position of the reaction locus is correspondingly smaller. On the other hand, if the matrix has large pores, then a fast advancement of CO_2(g) molecules is to be expected.

Quantity	*Definition*	*Dimension*	*Value*
D_5	Effective moisture diffusivity	cm^2 day^{-1}	1
D_3	Effective Ca(OH)$_2$(aq) diffusivity	cm^2 day^{-1}	0.864
D_2	Effective CO_2(aq) diffusivity	cm^2 day^{-1}	3.5
D_1	Effective CO_2(aq) diffusivity	cm^2 day^{-1}	0.62
λ_5	Initial values of moisture	g cm^{-3}	0.061
$\bar{c}$	Ambient concentration of CO_2(g)	g cm^{-3}	58.92×10^{-6}
$\hat{u}_{03}$	Initial value for Ca(OH)$_2$(aq)	g cm^{-3}	0.0775
s_0	Initial position of $\Gamma(t)$	cm	10^{-5}
$2L$	Length of the (observed) slab	cm	10
Q	Exchange factor in Henry's law	-	0.8227
P	Mass-transfer coefficient of CO_2(g)	day^{-1}	35760
$S_{3,diss}$	Factor in the dissolution law	day^{-1}	$\frac{1}{150}$
R	Gas constant	mol^{-1} K^{-1} atm	8206×10^{-5}
H	Henry's law constant for CO_2(g)	mol m^{-3}atm^{-1}	34.2
$\mathcal{M}_{CO_2}$	Molecular weight of CO_2	g mol^{-1}	44
$\mathcal{M}_{Ca(OH)_2}$	Molecular weight of Ca(OH)$_2$	g mol^{-1}	74

Table 2: Numerical data for parameters and input variables, [4].

Numerical ranges for many of the model parameters (like the effective diffusivity of each species, the reaction constants for carbonation and dissolution reactions, mass-transfer coefficients in Henry's law, etc.) and their correlation with significant material properties (like type of the cement, water-to-cement ratio, dependence of the total porosity on the carbonation-reaction rate, etc.) are only poorly known. However, despite of these inherent artifacts, the moving-interface approach provides a proper framework for further investigation of the right choice of the effective carbonation-reaction rate on the overall process.

5 Summary and conclusion

A two-phase moving-boundary system has been introduced to describe the penetration of the carbonation front, idealized as a sharp interface, into a concrete wall whose chemical composition and initial microstructure are known. The proposed model captures numerically most of the major features of the physico-chemical process. The shape and order of magnitude of the concentrations and their profiles, the high sensitivity with respect to the effective diffusion coeffi-

cient of gaseous CO_2 and the dominance of the reaction part against diffusive transport are pointed out. The simulations indicate a strong dependence of the output of the model on the choice of the parameters describing the carbonation-reaction rate. The computed penetration depths compare well with the measured penetration depths from [6]. Additionally, the computed concentration profiles are in the expected physical range.

Acknowledgments

This work was partially supported by the special priority program of DFG SPP 1122 *Prediction of the Course of Physicochemical Damage Processes Involving Mineral Materials*.

References

[1] V. Alexiades, A. D. Solomon, Mathematical Modeling of Melting and Freezing Processes, Hemisphere Publishing Group, Washington, Philadelphia, London, 1993.

[2] J. Bear, Dynamics of Fluids in Porous Media, Dover Publications Inc., N.Y., 1972.

[3] M. Böhm, J. Devinny, F. Jahani, G. Rosen, On a moving-boundary system modeling corrosion in sewer pipes, Appl. Math. Comput. 92 (1998) 247–269.

[4] M. Böhm, J. Kropp, A. Muntean, On a prediction model for concrete carbonation based on moving interfaces - Interface concentrated reactions, Berichte aus der Technomathematik 03-03, ZeTeM, University of Bremen (2003).

[5] M. Böhm, J. Kropp, A. Muntean, A two-reaction-zones moving-interface model for predicting $Ca(OH)_2$-carbonation in concrete, Berichte aus der Technomathematik 03-04, ZeTeM, University of Bremen (2003).

[6] D. Bunte, Zum karbonatisierungsbedingten Verlust der Dauerhaftigkeit von Außenbauteilen aus Stahlbeton, Ph.D. thesis, TU Braunschweig (1994).

[7] A. Caboussat, J. Rappaz, Analysis of a one-dimensional free boundary flow problem, Numer. Math. 101 (1) (2005) 67–86.

[8] T. Chaussadent, États de lieux et réflexions sur la carbonatation du beton armé, Technical report, Laboratoire Central de Ponts et Chaussées, Paris, 1999.

[9] J. N. Dewynne, A. C. Fowler, P. S. Hagan, Multiple reaction fronts in the oxidation-reduction of iron-rich uranium ores, SIAM J. Appl. Math. 53 (4) (1993) 971–989.

[10] G. F. Froment, K. B. Bischoff, Chemical Reactor Analysis and Design, 2nd Edition, Wiley Series in Chemical Engineering, John Wiley and Sons, NY, Chichester, Brisbane, Toronto, Singapore, 1990.

[11] A. Friedman, D. S. Ross, J. Zhang, A Stefan problem for a reaction-diffusion system, SIAM J. Math. Anal. 26 (1995) 1089–1112.

[12] A. Kharab, R. B. Guenther, A free boundary value problem for water invading an unsaturated medium, Computing 38 (1987) 185–207.

[13] M. E. Gurtin, Thermomechanics of Evolving Phase Boundaries in the Plane, Clarendon Press, Oxford, 1993.

[14] J. Kropp, Relations between transport characteristics and durability, in: J. Kropp, H. K. Hilsdorf (Eds.), Performance Criteria for Concrete Durability, RILEM Report 12, E and FN Spon Editions, 1995, pp. 97–137.

[15] S. Kutluay, Numerical schemes for one-dimensional Stefan-like problems with a forcing term, Appl. Math. Comput. 168 (2) (2005) 1159–1168.

[16] H. G. Landau, Heat conduction in a melting solid, Quart. Appl. Mech. Math. 8 (1950) 81–94.

[17] S. Larsson, V. Thomée, Partial Differential Equations with Numerical Methods, Springer Verlag, Berlin, Heidelberg, 2003.

[18] J. D. Logan, Transport Modeling in Hydrogeochemical Systems, Vol. 17 of Interdisciplinary Applied Mathematics, Springer Verlag, NY, Berlin, Heidelberg, Barcelona, Hong Kong, London, Milan, Paris, Singapore, Tokyo, 2001.

[19] K. Maekawa, T. Ishida, T. Kishi, Multi-scale modeling of concrete performance. integrated material and structural mechanics, Journal of Advanced Concrete Technology 1 (2) (2003) 91–126, Japan Concrete Institute.

[20] M. Mainguy, O. Coussy, Propagation fronts during calcium leaching and chloride penetration, ASCE J. Engng. Mech. 3 (2000) 252–257.

[21] S. A. Meier, M. A. Peter, M. Böhm, A two-scale modelling approach to reaction-diffusion processes in porous materials, accepted to Computational Material Sciences (2006).

[22] S. A. Meier, M. A. Peter, A. Muntean, M. Böhm, Modelling and simulation of concrete carbonation with internal layers, Berichte aus der Technomathematik 05-02, ZeTeM, University of Bremen (2005).

[23] A. M. Meirmanov, The Stefan Problem, Vol. 3 of De Gruyter Expositions in Mathematics, Walter de Gruyter, Berlin, NY, 1992.

[24] A. Muntean, M. Böhm, On a prediction model for the service life of concrete structures based on moving interfaces, in: F. Stangenberg, O. T. Bruhns, D. Hartmann, G. Meschke (Eds.), Proceedings of the Second International Conference Lifetime-Oriented Design Concepts, Ruhr-Universität Bochum, Germany, Bochum, 2004, pp. 209–218.

[25] A. Muntean, M. Böhm, Dynamics of a moving reaction interface in a concrete wall, in: J. F Rodrigues et al. (Eds.), Free and Moving Boundary Problems. Theory and Applications, Birkhäuser, Basel, 2006, in press.

[26] A. Muntean, A moving boundary problem: Modeling, analysis and simulation of concrete carbonation, Ph.D. thesis, ZeTeM, Faculty of Mathematics, University of Bremen, submitted (March 2006).

[27] P. J. Ortoleva, Geochemical Self-Organization, Vol. 23 of Oxford Monographs on Geology and Geophysics, Oxford University Press, NY, Oxford, 1994.

[28] V. G. Papadakis, C. G. Vayenas, M. N. Fardis, A reaction engineering approach to the problem of concrete carbonation, AIChE Journal 35 (1989) 1639.

[29] A. Pawell, K.-D. Krannich, Dissolution effects in transport in porous media, SIAM J. Appl. Math. 1 (1996) 89–118.

[30] A. Schmidt, A. Muntean, M. Böhm, Numerical experiments with self-adaptive finite element simulations in 2D for the carbonation of concrete, Berichte aus der Technomathematik 05-01, ZeTeM, University of Bremen (2005).

[31] A. Steffens, D. Dinkler, H. Ahrens, Modeling carbonation for corrosion risk prediction of concrete structures, Cement and Concrete Research 32 (2002) 935–941.

Berichte aus der Technomathematik ISSN 1435-7968

http://www.math.uni-bremen.de/zetem/berichte.html

— Vertrieb durch den Autor —

Reports **Stand: 26. April 2006**

98–01. Peter Benner, Heike Faßbender:
An Implicitly Restarted Symplectic Lanczos Method for the Symplectic Eigenvalue Problem, Juli 1998.

98–02. Heike Faßbender:
Sliding Window Schemes for Discrete Least-Squares Approximation by Trigonometric Polynomials, Juli 1998.

98–03. Peter Benner, Maribel Castillo, Enrique S. Quintana-Ortí:
Parallel Partial Stabilizing Algorithms for Large Linear Control Systems, Juli 1998.

98–04. Peter Benner:
Computational Methods for Linear–Quadratic Optimization, August 1998.

98–05. Peter Benner, Ralph Byers, Enrique S. Quintana-Ortí, Gregorio Quintana-Ortí:
Solving Algebraic Riccati Equations on Parallel Computers Using Newton's Method with Exact Line Search, August 1998.

98–06. Lars Grüne, Fabian Wirth:
On the rate of convergence of infinite horizon discounted optimal value functions, November 1998.

98–07. Peter Benner, Volker Mehrmann, Hongguo Xu:
A Note on the Numerical Solution of Complex Hamiltonian and Skew-Hamiltonian Eigenvalue Problems, November 1998.

98–08. Eberhard Bänsch, Burkhard Höhn:
Numerical simulation of a silicon floating zone with a free capillary surface, Dezember 1998.

99–01. Heike Faßbender:
The Parameterized SR Algorithm for Symplectic (Butterfly) Matrices, Februar 1999.

99–02. Heike Faßbender:
Error Analysis of the symplectic Lanczos Method for the symplectic Eigenvalue Problem, März 1999.

99–03. Eberhard Bänsch, Alfred Schmidt:
Simulation of dendritic crystal growth with thermal convection, März 1999.

99–04. Eberhard Bänsch:
Finite element discretization of the Navier-Stokes equations with a free capillary surface, März 1999.

99–05. Peter Benner:
Mathematik in der Berufspraxis, Juli 1999.

99–06. Andrew D.B. Paice, Fabian R. Wirth:
Robustness of nonlinear systems and their domains of attraction, August 1999.

99–07. Peter Benner, Enrique S. Quintana-Ortí, Gregorio Quintana-Ortí:
Balanced Truncation Model Reduction of Large-Scale Dense Systems on Parallel Computers, September 1999.

99–08. Ronald Stöver:
Collocation methods for solving linear differential-algebraic boundary value problems, September 1999.

99–09. Huseyin Akcay:
Modelling with Orthonormal Basis Functions, September 1999.

99–10. Heike Faßbender, D. Steven Mackey, Niloufer Mackey:
Hamilton and Jacobi come full circle: Jacobi algorithms for structured Hamiltonian eigenproblems, Oktober 1999.

99–11. Peter Benner, Vincente Hernández, Antonio Pastor:
On the Kleinman Iteration for Nonstabilizable System, Oktober 1999.

99–12. Peter Benner, Heike Faßbender:
A Hybrid Method for the Numerical Solution of Discrete-Time Algebraic Riccati Equations, November 1999.

99–13. Peter Benner, Enrique S. Quintana-Ortí, Gregorio Quintana-Ortí:
Numerical Solution of Schur Stable Linear Matrix Equations on Multicomputers, November 1999.

99–14. Eberhard Bänsch, Karol Mikula:
Adaptivity in 3D Image Processing, Dezember 1999.

00–01. Peter Benner, Volker Mehrmann, Hongguo Xu:
Perturbation Analysis for the Eigenvalue Problem of a Formal Product of Matrices, Januar 2000.

00–02. Ziping Huang:
Finite Element Method for Mixed Problems with Penalty, Januar 2000.

00–03. Gianfrancesco Martinico:
Recursive mesh refinement in 3D, Februar 2000.

00–04. Eberhard Bänsch, Christoph Egbers, Oliver Meincke, Nicoleta Scurtu:
Taylor-Couette System with Asymmetric Boundary Conditions, Februar 2000.

00–05. Peter Benner:
Symplectic Balancing of Hamiltonian Matrices, Februar 2000.

00–06. Fabio Camilli, Lars Grüne, Fabian Wirth:
A regularization of Zubov's equation for robust domains of attraction, März 2000.

00–07. Michael Wolff, Eberhard Bänsch, Michael Böhm, Dominic Davis:
Modellierung der Abkühlung von Stahlbrammen, März 2000.

00–08. Stephan Dahlke, Peter Maaß, Gerd Teschke:
Interpolating Scaling Functions with Duals, April 2000.

00–09. Jochen Behrens, Fabian Wirth:
A globalization procedure for locally stabilizing controllers, Mai 2000.

00–10. Peter Maaß, Gerd Teschke, Werner Willmann, Günter Wollmann:
Detection and Classification of Material Attributes – A Practical Application of Wavelet Analysis, Mai 2000.

00–11. Stefan Boschert, Alfred Schmidt, Kunibert G. Siebert, Eberhard Bänsch, Klaus-Werner Benz, Gerhard Dziuk, Thomas Kaiser:
Simulation of Industrial Crystal Growth by the Vertical Bridgman Method, Mai 2000.

00–12. Volker Lehmann, Gerd Teschke:
Wavelet Based Methods for Improved Wind Profiler Signal Processing, Mai 2000.

00–13. Stephan Dahlke, Peter Maass:
A Note on Interpolating Scaling Functions, August 2000.

00–14. Ronny Ramlau, Rolf Clackdoyle, Frédéric Noo, Girish Bal:
Accurate Attenuation Correction in SPECT Imaging using Optimization of Bilinear Functions and Assuming an Unknown Spatially-Varying Attenuation Distribution, September 2000.

00–15. Peter Kunkel, Ronald Stöver:
Symmetric collocation methods for linear differential-algebraic boundary value problems, September 2000.

00–16. Fabian Wirth:
The generalized spectral radius and extremal norms, Oktober 2000.

00–17. Frank Stenger, Ahmad Reza Naghsh-Nilchi, Jenny Niebsch, Ronny Ramlau:
A unified approach to the approximate solution of PDE, November 2000.

00–18. Peter Benner, Enrique S. Quintana-Ortí, Gregorio Quintana-Ortí:
Parallel algorithms for model reduction of discrete–time systems, Dezember 2000.

00–19. Ronny Ramlau:
A steepest descent algorithm for the global minimization of Tikhonov–Phillips functional, Dezember 2000.

01–01. Efficient methods in hyperthermia treatment planning:
Torsten Köhler, Peter Maass, Peter Wust, Martin Seebass, Januar 2001.

01–02. Parallel Algorithms for LQ Optimal Control of Discrete-Time Periodic Linear Systems:
Peter Benner, Ralph Byers, Rafael Mayo, Enrique S. Quintana-Ortí, Vicente Hernández, Februar 2001.

01–03. Peter Benner, Enrique S. Quintana-Ortí, Gregorio Quintana-Ortí:
Efficient Numerical Algorithms for Balanced Stochastic Truncation, März 2001.

01–04. Peter Benner, Maribel Castillo, Enrique S. Quintana-Ortí:
Partial Stabilization of Large-Scale Discrete-Time Linear Control Systems, März 2001.

01–05. Stephan Dahlke:
Besov Regularity for Edge Singularities in Polyhedral Domains, Mai 2001.

01–06. Fabian Wirth:
A linearization principle for robustness with respect to time-varying perturbations, Mai 2001.

01–07. Stephan Dahlke, Wolfgang Dahmen, Karsten Urban:
Adaptive Wavelet Methods for Saddle Point Problems - Optimal Convergence Rates, Juli 2001.

01–08. Ronny Ramlau:
Morozov's Discrepancy Principle for Tikhonov regularization of nonlinear operators, Juli 2001.

01–09. Michael Wolff:
Einführung des Drucks für die instationären Stokes–Gleichungen mittels der Methode von Kaplan, Juli 2001.

01–10. Stephan Dahlke, Peter Maaß, Gerd Teschke:
Reconstruction of Reflectivity Desities by Wavelet Transforms, August 2001.

01–11. Stephan Dahlke:
Besov Regularity for the Neumann Problem, August 2001.

01–12. Bernard Haasdonk, Mario Ohlberger, Martin Rumpf, Alfred Schmidt, Kunibert G. Siebert:
h–p–Multiresolution Visualization of Adaptive Finite Element Simulations, Oktober 2001.

01–13. Stephan Dahlke, Gabriele Steidl, Gerd Teschke:
Coorbit Spaces and Banach Frames on Homogeneous Spaces with Applications to Analyzing Functions on Spheres, August 2001.

02–01. Michael Wolff, Michael Böhm:
Zur Modellierung der Thermoelasto-Plastizität mit Phasenumwandlungen bei Stählen sowie der Umwandlungsplastizität, Februar 2002.

02–02. Stephan Dahlke, Peter Maaß:
An Outline of Adaptive Wavelet Galerkin Methods for Tikhonov Regularization of Inverse Parabolic Problems, April 2002.

02–03. Alfred Schmidt:
A Multi-Mesh Finite Element Method for Phase Field Simulations, April 2002.

02–04. Sergey N. Dachkovski, Michael Böhm:
A Note on Finite Thermoplasticity with Phase Changes, Juli 2002.

02–05. Michael Wolff, Michael Böhm:
Phasenumwandlungen und Umwandlungsplastizität bei Stählen im Konzept der Thermoelasto-Plastizität, Juli 2002.

02–06. Gerd Teschke:
Construction of Generalized Uncertainty Principles and Wavelets in Anisotropic Sobolev Spaces, August 2002.

02–07. Ronny Ramlau:
TIGRA – an iterative algorithm for regularizing nonlinear ill–posed problems, August 2002.

02–08. Michael Lukaschewitsch, Peter Maaß, Michael Pidcock:
Tikhonov regularization for Electrical Impedance Tomography on unbounded domains, Oktober 2002.

02–09. Volker Dicken, Peter Maaß, Ingo Menz, Jenny Niebsch, Ronny Ramlau:
Inverse Unwuchtidentifikation an Flugtriebwerken mit Quetschöldämpfern, Oktober 2002.

02–10. Torsten Köhler, Peter Maaß, Jan Kalden:
Time-series forecasting for total volume data and charge back data, November 2002.

02–11. Angelika Bunse-Gerstner:
A Short Introduction to Iterative Methods for Large Linear Systems, November 2002.

02–12. Peter Kunkel, Volker Mehrmann, Ronald Stöver:
Symmetric Collocation for Unstructured Nonlinear Differential-Algebraic Equations of Arbitrary Index, November 2002.

02–13. Michael Wolff:
Ringvorlesung: Distortion Engineering 2
Kontinuumsmechanische Modellierung des Materialverhaltens von Stahl unter Berücksichtigung von Phasenumwandlungen, Dezember 2002.

02–14. Michael Böhm, Martin Hunkel, Alfred Schmidt, Michael Wolff:
Evaluation of various phase-transition models for 100Cr6 for application in commercial FEM programs, Dezember 2002.

03–01. Michael Wolff, Michael Böhm, Serguei Dachkovski:
Volumenanteile versus Massenanteile - der Dilatometerversuch aus der Sicht der Kontinuumsmechanik, Januar 2003.

03–02. Daniel Kessler, Ricardo H. Nochetto, Alfred Schmidt:
A posteriori error control for the Allen-Cahn Problem: circumventing Gronwall's inequality, März 2003.

03–03. Michael Böhm, Jörg Kropp, Adrian Muntean:
On a Prediction Model for Concrete Carbonation based on Moving Interfaces - Interface concentrated Reactions, April 2003.

03–04. Michael Böhm, Jörg Kropp, Adrian Muntean:
A Two-Reaction-Zones Moving-Interface Model for Predicting $Ca(OH)_2$ Carbonation in Concrete, April 2003.

03–05. Vladimir L. Kharitonov, Diederich Hinrichsen:
Exponential estimates for time delay systems, May 2003.

03–06. Michael Wolff, Michael Böhm, Serguei Dachkovski, Günther Löwisch:
Zur makroskopischen Modellierung von spannungsabhängigem Umwandlungsverhalten und Umwandlungsplastizität bei Stählen und ihrer experimentellen Untersuchung in einfachen Versuchen, Juli 2003.

03–07. Serguei Dachkovski, Michael Böhm, Alfred Schmidt, Michael Wolff:
Comparison of several kinetic equations for pearlite transformation in 100Cr6 steel,
Juli 2003.

03–08. Volker Dicken, Peter Maass, Ingo Menz, Jenny Niebsch, Ronny Ramlau:
Nonlinear Inverse Unbalance Reconstruction in Rotor dynamics,
Juli 2003.

03–09. Michael Böhm, Serguei Dachkovski, Martin Hunkel, Thomas Lübben, Michael Wolff:
Übersicht über einige makroskopische Modelle für Phasenumwandlungen im Stahl,
Juli 2003.

03–10. Michael Wolff, Friedhelm Frerichs, Bettina Suhr:
Vorstudie für einen Bauteilversuch zur Umwandlungsplastizität bei der perlitischen Umwandlung des Stahls 100 Cr6,
August 2003.

03–11. Michael Wolff, Bettina Suhr:
Zum Vergleich von Massen- und Volumenanteilen bei der perlitischen Umwandlung der Stähle 100Cr6 und C80,
September 2003.

03–12. Rike Grotmaack, Adrian Muntean:
Stabilitätsanalyse eines Moving-Boundary-Modells der beschleunigten Karbonatisierung von Portlandzementen,
September 2003.

03–13. Alfred Schmidt, Michael Wolff, Michael Böhm:
Numerische Untersuchungen für ein Modell des Materialverhaltens mit Umwandlungsplastizität und Phasenumwandlungen beim Stahl 100Cr6 (Teil 1),
September 2003.

04–01. Liliana Cruz Martin, Gerd Teschke:
A new method to reconstruct radar reflectivities and Doppler information,
Januar 2004.

04–02. Ingrid Daubechies, Gerd Teschke:
Wavelet based image decomposition by variational functionals,
Januar 2004.

04–03. N. Guglielmi, F. Wirth, M. Zennaro:
Complex polytope extremality results for families of matrices,
März 2004.

04–04. I. Daubechies, G. Teschke:
Variational image restoration by means of wavelets: simultaneous decomposition, deblurring and denoising,
April 2004.

04–05. V.L. Kharitonov, E. Plischke:
Lyapunov matrices for time-delay systems,
April 2004.

04–06. Ronny Ramlau:
On the use of fixed point iterations for the regularization of nonlinear ill-posed problems,
Juni 2004.

04–07. Christof Büskens, Matthias Knauer:
Higher Order Real-Time Approximations In Optimal Control of Multibody-Systems For Industrial Robots,
August 2004.

04–08. Christof Büskens, Roland Griesse:
Computational Parametric Sensitivity Analysis of Perturbed PDE Optimal Control Problems with State and Control Constraints,
August 2004.

04–09. Christof Büskens:
Higher Order Real-Time Approximations of Perturbed Control Constrainted PDE Optimal Control Problems ,
August 2004.

04–10. Christof Büskens, Matthias Gerdts:
Differentiability of Consistency Functions,
August 2004.

04–11. Robert Baier, Christof Büskens, Ilyes Aïssa Chama, Matthias Gerdts:
Approximation of Reachable Sets by Direct Solution Methods of Optimal Control Problems,
August 2004.

04–12. J. Soares, G. Teschke, M. Zhariy:
A Wavelet Regularization for Nonlinear Diffusion Equations,
September 2004.

05–01. Alfred Schmidt, Adrian Muntean, Michael Böhm:
Numerical experiments with Self-Adaptive Finite Element Simulations in 2D for the Carbonation of Concrete,
April 2005.

05–02. Sebastian A. Meier, Malte A. Peter, Adrian Muntean, Michael Böhm:
Modelling and simulation of concrete carbonation with internal layers,
April 2005.

05–03. Malte A. Peter, Adrian Muntean, Sebastian A. Meier, Michael Böhm:
Modelling and simulation of concrete carbonation: competition of several carbonation reactions,
April 2005.

05–04. Adrian Muntean, Sebastian A. Meier, Malte A. Peter, Michael Böhm, Jörg Kropp:
A note on limitations of the use of accelerated concrete-carbonation tests for service-life predictions,
April 2005.

05–05. Sergey Dashkovskiy, Björn S. Rüffer, Fabian R. Wirth:
An ISS Small-Gain Theorem for General Networks,
Juni 2005.

06–01. Prof. Dr. Christof Büskens, Peter Lasch:
Suboptimal Improvement of the classical Riccati Controller,
März 2006.

06–02. Michael Wolff, Michael Böhm:
Transformation-induced plasticity in steel - general modelling, analysis and parameter identification,
April 2006.

06–03. Adrian Muntean, Michael Böhm:
A sharp-interface moving-boundary system modeling carbonation penetration in concrete, April 2006.